BJES Basrah Journal for Engineering Sciences

Basrah Journal for Engineering Sciences, Vol. 24, No. 2, (2024), 43-49

Original Article

Journal homepage: www.bjes.edu.iq
ISSN (Online): 23118385, ISSN (Print): 18146120

Simulation of Flow Around Circular Cylinders for Complex von Kármán Vortex Street Phenomenon Using SIMPLE, SIMPLEC and PISO

Ali K. Hadi [1]*, Rafid J. Mohammed [2], Qahtan A. Jawad [3], Imad A. Kheioon [4]

[1,2,3,4] *Department of Mechanical Engineering, College of Engineering, University of Basrah, Basrah, Iraq*

E-mail addresses: ali.k.hadi @uobasrah.edu.iq , rafid.mohammed@uobasrah.edu.iq , qahtan.jawad@uobasrah.edu.iq , imad.kheioon@uobasrah.edu.iq

Received: 5 June 2024; Accepted: 6 August 2024; Published: 17 August 2024

Abstract

Van Kármán vortex street is considered an important phenomenon that accompanies fluid flow, especially when exposed to a certain barrier, as periodic vortexes occur on both sides of the body that rotate in two opposite directions. This phenomenon occurs in the atmosphere around mountains, oceans, seas, and islands. Also, this phenomenon makes it possible to induce a fluid flow around a specific body present in the flow path. In this study, a model for fluid flow around a cylinder of a certain diameter was taken, where the flow near the boundary layers of the cylinder surface moves slower than near the free stream. In addition, the pressure distribution was studied, and it was observed that there is a pressure gradient due to the difference in momentum at the surface of the cylinder in distant areas due to friction. The study area was divided into fine meshes with Fluent software, especially in the irregular areas. The simulation was implemented for Reynolds numbers Re = 100 and Re = 1500 for incompressible flows. Consequently, the equations that do not depend on pressure are difficult to solve. Therefore, methods linking pressure and velocity were adopted, where the pressure-velocity coupling simple method was used. The first-order forward difference scheme was adopted in representing the differential equations as a function of time when performing the simulation. From the steady state and upwards to Reynolds number Re = 100, it was observed that a twain of vortices appeared on the body at a certain speed range. When the state was changed from the stable state to the transitional state, the results changed, as the flow became asymmetric and unsteady due to vortex shedding phenomena, which led to the generation of vortexes in different ways. The U-Velocity curve was studied for two different cases, and the results showed a large discrepancy between the first order and the second order, where the second order had better behavior but required great effort to reach accurate results. Also, pressure-velocity was studied to satisfy mass conservation, and numerical techniques were used to compute the equations of Navier-Stokes in CFD, such as SIMPLEC, PISO, and SIMPLE. An acceptable convergence was not reached with the PISO; therefore, the SIMPLE method was adopted. The pressure gradient was drawn around the cylinder, where it was observed that the pressure was greatest at the front of the cylinder and its lowest value at the end.

Keywords: von Kármán vortex street, Reynolds number, Vortex shedding phenomena, SIMPLE, SIMPLEC, PISO.

http://doi.org/10.33971/bjes.24.2.6

1. Introduction

Von Kármán vortex is a complex phenomenon in fluid mechanics, seen in many places. Vortices rotate in opposite directions from object sides. Common examples of the phenomenon in civil engineering include the structural dynamics of skyscrapers, chimney stacks, the atmosphere around mountains, suspension bridges, marine engineering, which includes the vibrations of pipelines resting in the seabed, and ocean engineering, as shown in Fig. 1 [1].

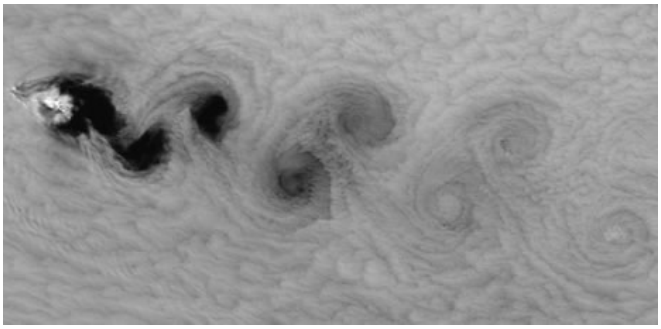

Fig. 1 von Kármán Vortex around an island on the sea [2].

Many researchers have been investigated in this field as will be reviewed by the following survey.

Gupta [3] introduced a new method to identify the vortex-shedding parameters. A wind-tunnel tests on two objectives, the first was a circular cylinder and the second was two bridge decks configuration. The author estimated the response of vortex-induced by determining the model parameters from the experiments.

Tapia and Chellali [4] developed a simplified model of Kármán Street by CFD simulations. They used this model to train neural network-based controllers of different robot fishes in order to control the frequency of fishes' tail beat before releasing them into water. They deduced that frequency of fishes' tail beat was well matched with Kármán Street.

Thoraval et al. [5] studied the irregular splashing which result from impinging a drop on a liquid pool. They used super-speed video technology in conjunction with numerical simulations of high accuracy to display the irregular splashing. They reported that, at higher Reynolds numbers, an axisymmetric von Kármán vortex was shed from the free surface into the liquid. Ali et al. [6] Numerically investigated a flexible flap that generated vortices in an environment of

laminar flow to improve the performance of some kinds of heat exchangers. They used a square cylinder in 2D domain like generate a von Kármán vortex street. They concluded that vortices generated by each individual flap will induce a motion perturbation on the close flap leading the oscillations to be self-sustained. Noor [7] performed a numerical simulation of different bluff body shapes, such as triangular, rectangular, and circular, to study the vortex-shedding phenomenon. The author observed that to obtain better performance, the vortex flow meter must have sharp corner to produce vortex shedding frequency with stable value.

Wang and Alben [8] developed a numerical model to study the vortex streets dynamics when flowing in channel. The reverse and regular von Karmen streets with different geometries, Reynolds numbers (*Re*), and strengths were studied. They deduced that inflow vortex street was kept for the reverse von Kármán and changed for the regular street. They noticed for regular streets, that a transition to nonsymmetric dynamics is occurred when vortices are powerful, or (*Re*) rises, or vortex streets are extended vertically or compressed horizontally. Dol [9] conducted a turbulence investigation in a rotating circular cylinder wake in a free uniform stream to describe the vortex shedding patterns up to inhibition of the periodic vortex street of high-speed ratios. The author established that Kármán Vortices shedding in the generated wake was amended by rotating of the cylinder. Heil et al. [10] analyzed the 2D flow past a circular cylinder to explain the alterations in the field of vorticity topology that resulted in the creation of the von Kármán vortex. They demonstrated that as Reynolds number increases, the points of vortices formation and vanishing move fast downstream and upstream, respectively. Dai et al. [11] the investigation focused on the inhibition of vortex shedding, considering two key parameters: the width ratio of the splitter plate and the height-to-diameter ratio of the cylinder, as well as the length. They deduced that the splitter-plate supplied an effective and feasible procedure for vortex hindrance at a high *Re*, and the degree of inhibition can be greatly increased by an optimum configuration. Morast [12] used multi-layer perceptron and convolutional neural networks (CNN) to analyze the different structures formed in von Kármán vortex street in order to determine Reynolds number that governing the fluid flow system. The author concluded that deep learning algorithms (neural networks) can be learn the parameterization of Navier-Stokes equations from von Kármán vortex street and foresee the object locations. Greco et al. [13] used a synthetic jet technology represented by a slot in the rear of an open wind tunnel to discuss the von Kármán vortex behind a cylinder. The effects of dimensionless frequency and momentum coefficient on behavior of von Kármán Street were studied. Ghazijahani et al. [14] conducted echo state networks in order to predict the velocity fields in von Kármán vortex street by aiding of Particle Image Velocimetry (PIV) data. Maches et al. [15] investigated the stability and existence of von Kármán vortex street consisted of regular clusters similar to polygonal-shape represented by spatially periodic vortices. They captured the infinite vortex streets stability by using a point-vortex model. Alzabari et al. [16] used the simulation of large-eddy to investigate the turbulent flow created by a horizontal cylinder on the free surface, which was increasingly shallow with ratios of submergence-to-cylinder diameter between 0.5 and 2.1.

Keeler and Crowdy [17] achieved a new exact solution to the problem of steadily traveling with the 2D vorticity of water waves.

In the present study, the impact of a high Reynolds number (*Re*) on the field of flow of the von Kármán vortex and hydrodynamic instability will be investigated.

2. Methodology

The unsteady flow of a fluid over bluff bodies results in a repeating pattern of swirling vortices, which causes a von Kármán vortex. The flow near the boundary layers in a circular cylinder moves slower than the flow near the free stream. The flow momentum near of the cylinder surface is low because the viscous effects create a pressure gradient. Pressure gradient regions cause the separation of flow at points along the body. When flow separation occurs, the flow changes into swirling eddies, creating a wake region, as shown in Fig. 2 [18].

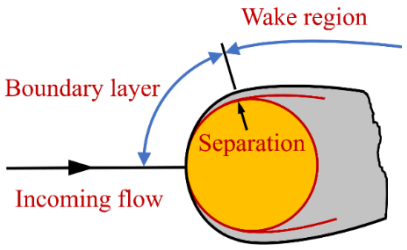

Fig. 2 Boundary layer around cylinder.

The vortices start to form in the laminar flow at a low Reynolds number between 5 and 40, and when increases above 40, the wake becomes unstable and vortex shedding starts to appear. One vortex becomes larger relative to another. When the bigger vortex gets powerful enough, the opposing vortex is drawn over the weaker one, where vortex A rotates clockwise, while the opposite vortex B rotates counterclockwise. The vortex B will not allow further supply of vortices to the vortex A, leading to shedding the vortex A. Following vortex A, a new vortex, namely vortex C, will form on the same side, which will get rid of vortex B. Every time, this process will continue when one side sheds a new vortex, as shown in Fig. 3 [19].

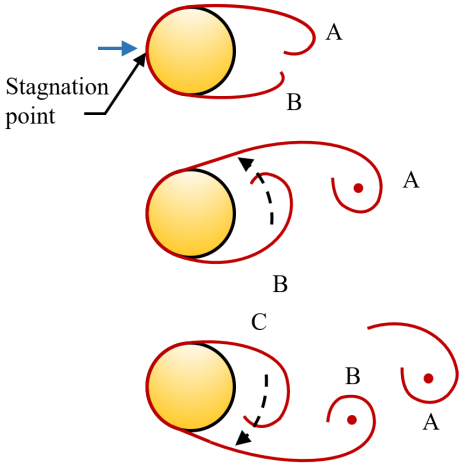

Fig. 3 von Kármán Vortex development.

The dimensionless Strouhal number (St) describes the frequency of vortex shedding. The Strouhal number normalizes the frequency of vortex shedding (f_s) with the cylinder diameter (D) and flow velocity (u).

$$St = \frac{f_s D}{u} \quad (1)$$

With an increasing Reynolds number, the laminar flow undergoes a turbulent transition over 300-400, the vortex periodicity does not occur, turbulence develops, and thus the von Kármán vortex totally disappears. The vortex shedding appears at Re near 40, and the Strouhal number is at 0.1. The Strouhal number increases to 0.2 and stays constant when the Reynolds number increases [20].

1. Mathematical and Numerical Formulation

The SIMPLE, SIMPLEC, and PISO algorithms commonly employ numerical techniques to compute the Navier-Stokes equations in the CFD, as shown in Fig. 4.

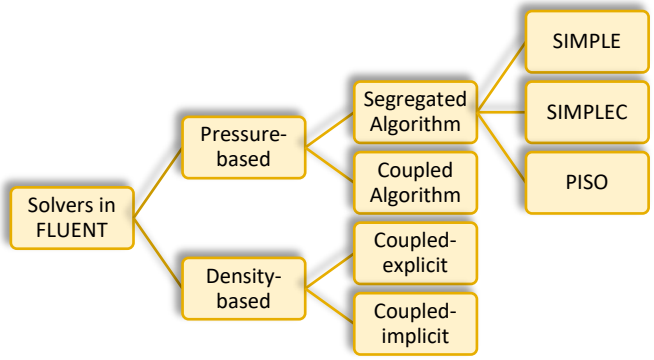

Fig. 4 Flow chart for the SIMPLE, SIMPLEC, and PISO algorithms to compute the Navier-Stokes equations.

SIMPLE algorithm

The algorithm of the semi-implicit method can be summarized in Fig. 5:

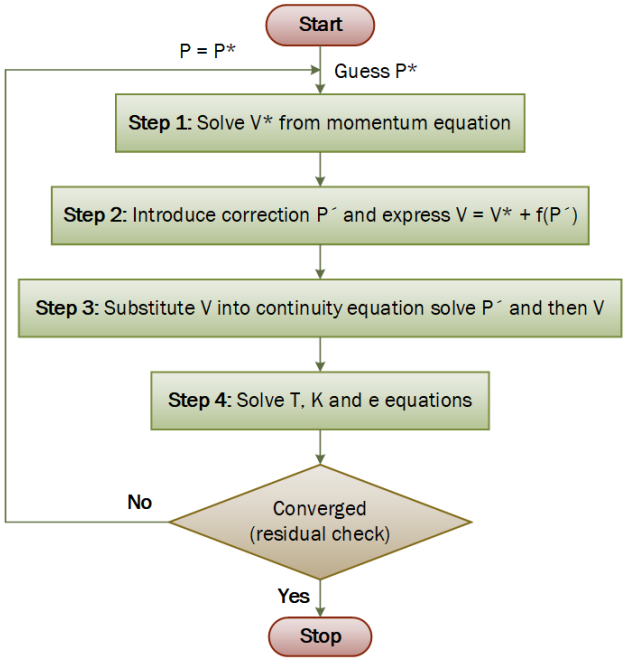

Fig. 5 Algorithm of the Semi-implicit Method (SIMPLE).

SIMPLEC algorithm

The SIMPLEC is a modified version of the SIMPLE algorithm that follows the same steps and algorithm. As a result, momentum equations are modified to omit less significant terms from velocity correction equations than those omitted in SIMPLE. This adjustment aims to reduce the impact of neglecting velocity neighbor correction terms. Figure 6 shows the implicit pressure-based scheme for the Navier-Stokes equations (SIMPLEC).

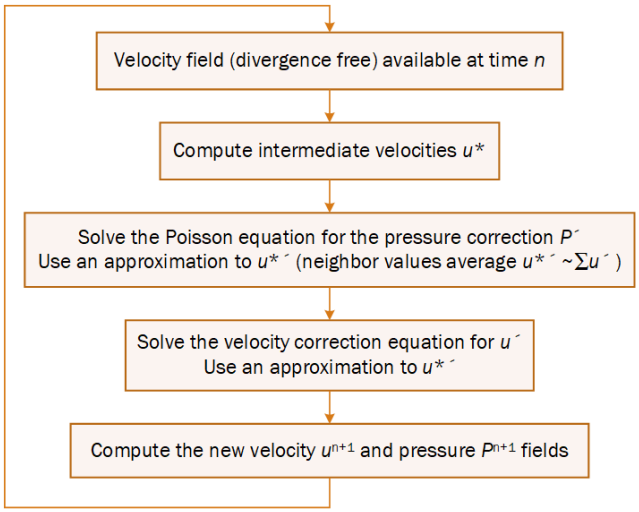

Fig. 6 The implicit pressure-based scheme for the Navier-Stokes equations.

PISO algorithm

The Pressure-Implicit with Splitting of Operators (PISO) algorithm is an extension method for the SIMPLE algorithm. PISO has been successfully adapted for steady-state problems as well. This pressure-velocity calculation procedure uses two corrector steps and one predictor step to ensure mass conservation, as shown in Fig. 7.

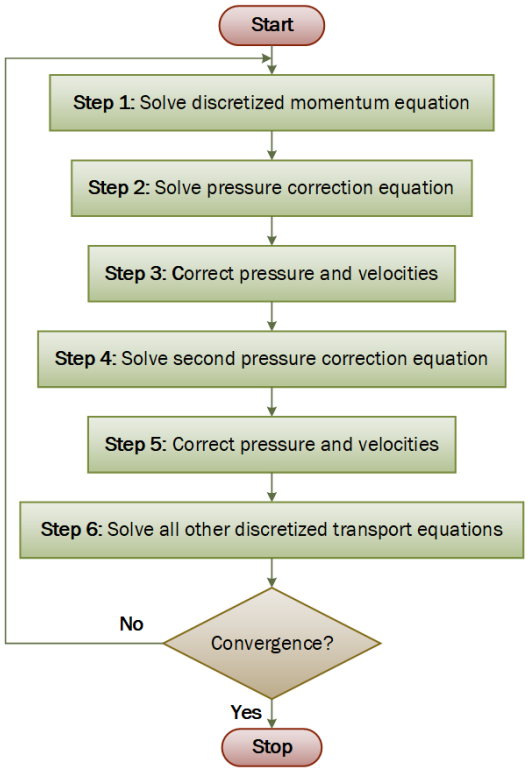

Fig. 7 The algorithm Pressure-Implicit with Splitting of Operators (PISO).

The governing Navier-Stokes equations are considered in a two-dimensional system of flow and are written for turbulence flow. Thus, the Reynolds Averaged Navier Stokes (RANS) equations are used. The governing equations that describe the problem are written as [21]:

Conservation of mass:

$$\frac{\partial \overline{u}_i}{\partial x_i} + \frac{\partial \overline{u}_i}{\partial y_i} = 0 \tag{2}$$

Conservation of momentum:

$$\frac{\partial \overline{u}_i}{\partial t} + \overline{u}_j \frac{\partial \overline{u}_i}{\partial x_j} = -\frac{1}{\rho}\left(\frac{\partial p}{\partial x_i}\right) + \vartheta\left(\frac{\partial^2 u_i}{\partial x_j^2}\right) - \frac{\partial \overline{\acute{u}_i \acute{u}_j}}{\partial x_j} \tag{3}$$

The flow assumed is incompressible; therefore, the Mach number is lower than 0.3, and the solution of the governing equation is missing the independent equation for pressure. Thus, the pressure-velocity coupling SIMPLE method is used in order to link pressure and velocity.

The equations 2 and 3 have been solved with the finite volume method, featuring a second-order upwind spatial discretization. The unsteady simulation used the second-order implicit method.

The time derivative is discretized by applying the first-order forward difference scheme. From Taylor expansion:

$$\overline{U_j^{n+1}} = \overline{U_j^n} + \Delta t\left(\frac{\partial \overline{U}}{\partial t}\right)_j^n + \frac{\Delta t^2}{2!}\left(\frac{\partial^2 \overline{U}}{\partial t^2}\right)_j^n + \frac{\Delta t^3}{3!}\left(\frac{\partial^3 \overline{U}}{\partial t^3}\right)_j^n + \text{H.O.T.}$$

$$\left(\frac{\partial \overline{U}}{\partial t}\right)_j^n = \frac{\overline{U_j^{n+1}} - \overline{U_j^n}}{\Delta t} - \frac{\Delta t^2}{2!}\left(\frac{\partial^2 \overline{U}}{\partial t^2}\right)_j^n - \frac{\Delta t^3}{3!}\left(\frac{\partial^3 \overline{U}}{\partial t^3}\right)_j^n - \text{H.O.T.}$$

$$\left(\frac{\partial \overline{U}}{\partial t}\right)_j^n = \frac{\overline{U_j^{n+1}} - \overline{U_j^n}}{\Delta t} + \text{O}(\Delta t) \tag{4}$$

The advection part of the momentum conservation can be discretized as the time derivative part (local acceleration).

$$\left(\frac{\partial \overline{U}}{\partial x}\right)_j^n = \frac{\overline{U_{j+1}^n} - \overline{U_j^n}}{\Delta x} + \text{O}(\Delta x) \tag{5}$$

The pressure gradient is discretized as the previous part.

$$\frac{1}{\rho}\left(\frac{\partial P}{\partial x}\right)_j^n = \frac{1}{\rho}\frac{P_{j+1}^n - P_{j-1}^n}{2\Delta x} + \text{O}(\Delta x^2) \tag{6}$$

Discretization of diffusion equations in the second-order finite difference in space by a centered scheme.

From Taylor expansion:

$$\overline{U_{j+1}^n} = \overline{U_j^n} + \Delta x\left(\frac{\partial \overline{U}}{\partial x}\right)_j^n + \frac{\Delta x^2}{2!}\left(\frac{\partial^2 \overline{U}}{\partial x^2}\right)_j^n + \frac{\Delta x^3}{3!}\left(\frac{\partial^3 \overline{U}}{\partial x^3}\right)_j^n + \frac{\Delta x^4}{4!}\left(\frac{\partial^4 \overline{U}}{\partial x^4}\right)_j^n + \text{H.O.T.} \tag{7}$$

$$\overline{U_{j-1}^n} = \overline{U_j^n} - \Delta x\left(\frac{\partial \overline{U}}{\partial x}\right)_j^n + \frac{\Delta x^2}{2!}\left(\frac{\partial^2 \overline{U}}{\partial x^2}\right)_j^n - \frac{\Delta x^3}{3!}\left(\frac{\partial^3 \overline{U}}{\partial x^3}\right)_j^n + \frac{\Delta x^4}{4!}\left(\frac{\partial^4 \overline{U}}{\partial x^4}\right)_j^n + \text{H.O.T.} \tag{8}$$

Summing the previous equations.

$$\overline{U_{j+1}^n} + \overline{U_{j-1}^n} = 2\overline{U_j^n} + 2\frac{\Delta x^2}{2!}\left(\frac{\partial^2 \overline{U}}{\partial x^2}\right)_j^n + 2\frac{\Delta x^4}{4!}\left(\frac{\partial^4 \overline{U}}{\partial x^4}\right)_j^n + \text{H.O.T}$$

$$\left(\frac{\partial^2 \overline{U}}{\partial x^2}\right)_j^n = \frac{\overline{U_{j+1}^n} - 2\overline{U_j^n} + \overline{U_{j-1}^n}}{\Delta x^2} - 2\frac{\Delta x^4}{4!}\left(\frac{\partial^4 \overline{U}}{\partial x^4}\right)_j^n + \text{H.O.T}$$

$$\left(\frac{\partial^2 \overline{U}}{\partial x^2}\right)_j^n = \frac{\overline{U_{j+1}^n} - 2\overline{U_j^n} + \overline{U_{j-1}^n}}{\Delta x^2} + \text{O}(\Delta x^4) \tag{9}$$

The discretized equation can be written as follows:

Conservation of mass:

$$\left(\frac{\partial \overline{U}}{\partial x}\right)_j^n = \frac{\overline{U_{j+1}^n} - \overline{U_j^n}}{\Delta x} + \text{O}(\Delta x) \tag{10}$$

Conservation of momentum:

$$\frac{\overline{U_j^{n+1}} - \overline{U_j^n}}{\Delta t} - \frac{\overline{U_{j+1}^n} - \overline{U_j^n}}{\Delta x} + \frac{1}{\rho}\frac{P_{j+1}^n - P_j^n}{\Delta x} - \frac{\overline{U_{j+1}^n} - 2\overline{U_j^n} + \overline{U_{j-1}^n}}{\Delta x^2} + \text{O}(\Delta t, \Delta x, \Delta x^4) \tag{11}$$

The discretization with the finite volume method could be done as follows:

$$\left(\frac{\partial \overline{U}}{\partial x}\right)_j^n = \frac{1}{\Delta V}\int_V \frac{\partial \overline{U}}{\partial x}\, dV = \frac{1}{\Delta V}\int_A \overline{U} dA = \frac{1}{\Delta V}\sum_{i=1}^{N} \overline{U} A$$

$$\left(\frac{\partial^2 \overline{U}}{\partial x^2}\right)_j^n = \frac{1}{\Delta V}\int_V \frac{\partial^2 \overline{U}}{\partial x^2}\, dV = \frac{1}{\Delta V}\int_A \frac{\partial \overline{U}}{\partial x} dA = \frac{1}{\Delta V}\sum_{i=1}^{N} \frac{\partial \overline{U}}{\partial x} A$$

The resulting system of linear algebraic equations is not tridiagonal because we have 6 unknown variables, and thus direct methods are more suitable, for example, Guess-Jordan elimination or the *LU* factorization method.

The flow is characterized in a Cartesian coordinate system with two dimensions (x, y), where the x-axis is aligned with the direction of the inlet flow and the y-axis is parallel to the axis of the cylinder.

The mesh should be able to catch all the flow details behind the cylinder. The size of the computational domain is $60D \times 25D$ with the cylinder circle at a distance of $10D$ from the inlet of the domain. The boundary layers are defined so that the inlet is located at $10D$ from the cylinder, while the outlet is placed at $50D$ from the cylinder. The cylinder diameter is $D = 0.1$ m, as shown in Fig. 8.

The following assumptions have been adopted:

- The inlet velocity U in the computational domain is uniform.
- For the domain walls, the no-slip condition is applied, $U_{walls} = 0$.
- The flow Reynolds number is 100.

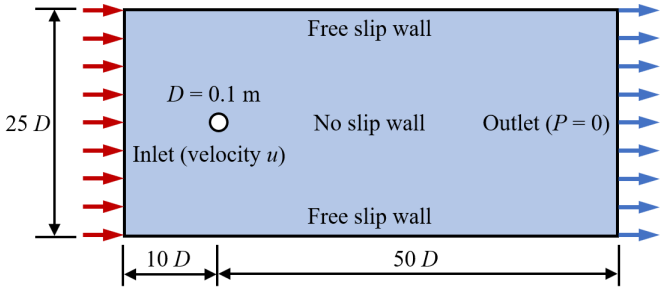

Fig. 8 Mesh boundary conditions.

It is important to get accurate results in the simulation. Therefore, the refinement mesh structure is used around the cylinder, as shown in Fig. 9. One factor that affects the accuracy of the simulations is the convergence value, which is defined in the Fluent simulation software. It should be small enough to thrust the numerical calculations. In simulations, the convergence criteria were selected as 10^{-6}. Simulations require fine meshes, especially in regions with high gradients. If the results change when the number of cells is changed while solving the simulation, it means that the mesh is not working properly. In this case, having 1,200,000 structured meshes resulted in an independent mesh. Time steps in various Reynolds numbers were computed using the current number, and the time steps that were less than this number were implemented in the software. When the Reynolds number is 100, the time step is 0.1, and when the Reynolds number is 1500, the time step is 0.05.

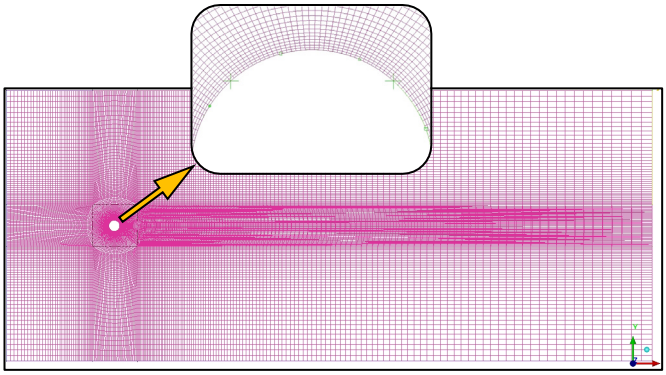

Fig. 9 Region of fine simulation mesh with a high gradient.

2. Results and Discussion

The simulation started with steady-state and continued to transient conditions. The simulations were performed with two different Reynolds numbers: Re = 100 and Re = 1500. Figure 10 shows the velocity field around the cylinder in the steady state. As this simulation was performed in a steady state, there are almost a pair of vortices in the back of the bluff body.

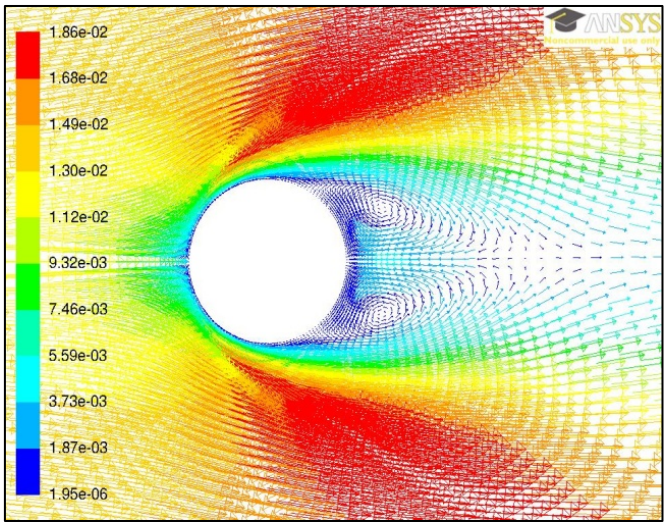

Fig. 10 Steady-state simulation for Re = 100.

When the steady-state simulations continue into the transition mode, the results will change. Figure 11 shows the transient results for Re = 100. Figure 9 shows the flow over the cylinder is not symmetric and steady. This is because of vortex-shedding phenomena, which cause the vortices to grow differently. The cylinder top and bottom form pairs of eddies alternately, creating vortex shedding as they travel to the wake region.

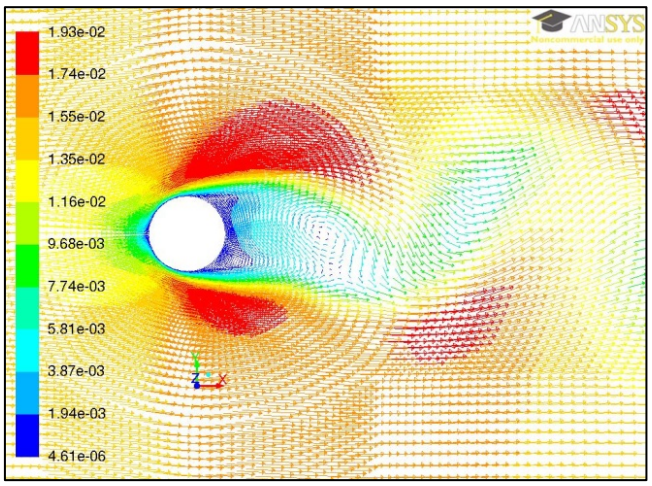

Fig. 11 Transition simulation for Re = 100.

Figure 12 shows the U-velocity profile along the centerline for two different simulations. Also, the graph shows there is a significant discrepancy between the first-order and second-order results upstream, which affects the accuracy of the results. Second-order discretization is proposed, but more efforts should be made to be certain about the accuracy of the results.

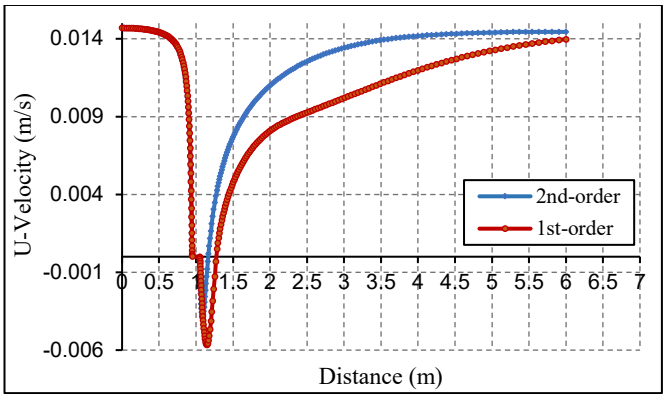

Fig. 12 U-velocity profile along the centerline for *Re* = 100.

Fluent Simulation software uses three different methods to couple pressure and velocity: SIMPLE, SIMPLEC, and PISO. In this work, SIMPLE and PISO were implemented. The PISO method did not converge for continuity equations, and as mentioned before, the SIMPLE method was used. Figure 13 shows Pressure distribution over the cylinder, with maximum pressure at the front of the cylinder (angles 0° or 360°) and minimum in the back (90° or 270°). At any point on the surface of the cylinder, the fluid has two components: Pressure is normal to the surface, while shear stress is tangential. The tangential pressure gradient along the cylinder surface generates a vortex behind the cylinder. The flow momentum is quite low near the surface of the cylinder due to viscous effects [2]. Furthermore, the pressure tangential component of acceleration is another mechanism that affects the front and rear surfaces of the oscillating cylinder but not the upper or lower surfaces. When the cylinder accelerates downward, it produces fluxes of CW vorticity on the front face of the cylinder and CWW vorticity on the rear face of the cylinder.

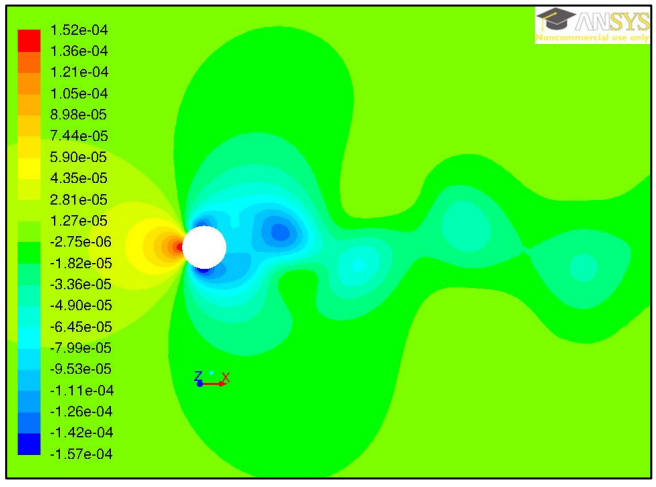

Fig. 13 Pressure distribution over the cylinder.

Figures 14 and 15 show the drag and lift coefficients for the cylinder in different time steps for *Re* = 1500. When a vortex is dropped from the top, a low-pressure area is created, and the cylinder is subjected to the lift force. Another vortex is created after half a cycle at the bottom, leading to lift force changes.

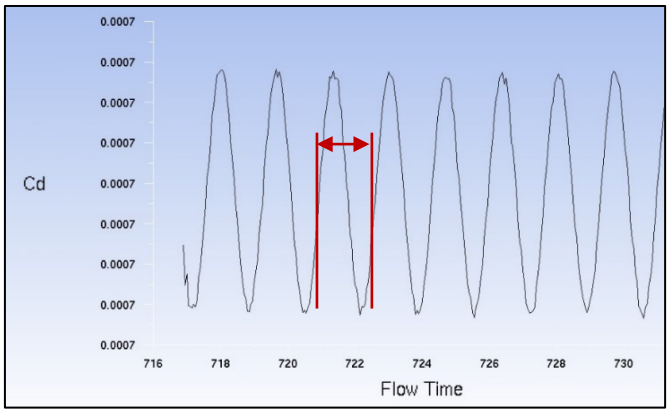

Fig. 14 Lift coefficient changes during time steps.

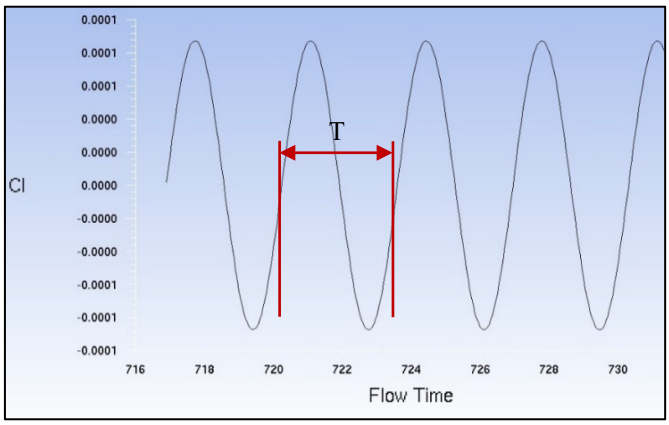

Fig. 15 Drag coefficient changes during time steps.

Figure 16 shows the velocity profile for two different turbulence models. Very close agreement downstream and at a short distance after the cylinder was observed. But in the wake region, the results were different.

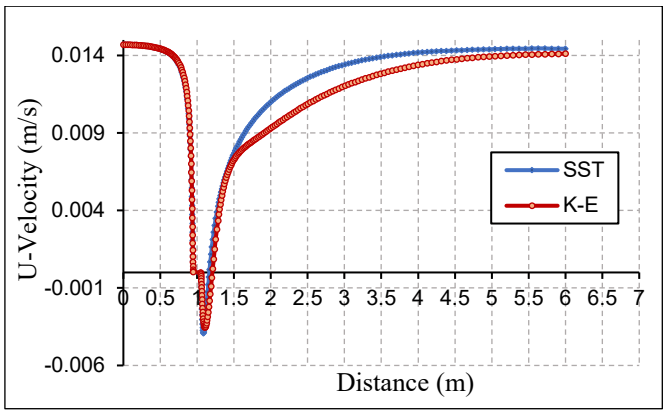

Fig. 16 U-Velocity profile for two different turbulence models.

Conclusions

Kármán vortex street is a phenomenon in fluid mechanics that occurs in a flowing fluid when it passes over a body. These vortexes occur alternately behind the body and are called the Kármán vortex street.

In the current case, the body is assumed to be a cylinder. As the fluid passes over it at a certain speed, it is possible to deduce different shapes for the vortices emerging behind the

cylinder. Additionally, the formation of vortexes can be controlled by the Reynolds number.

In this work, the flow around the cylinder was discussed theoretically. The governing equations were presented, and the model was simulated in Fluent software. Different parameters, such as pressure, U-velocity profile, drag, and lift coefficients, were investigated. Simulation of the flow with two turbulent models had very close results for u-velocity along the centerline. Regarding the accuracy of the results, although it was tried to increase the accuracy of the simulations, more efforts are needed to validate the results.

References

[1] F. C. Lombardi, A. Bongarzone, G. A. Zampogna, F. Gallaire, S. Camarri, and P. G. Ledda, "Von Kármán vortex street past a permeable circular cylinder: Two-dimensional flow and dynamic-mode-decomposition-based secondary stability analysis," Physical Review Fluids, Vol. 8, Issue 8, 2023. https://doi.org/10.1103/PhysRevFluids.8.083901

[2] http://community.tigranetworks.co.uk/blogs/tim_long/

[3] H. Gupta, "A new approach for identification of vortex-shedding parameters in time domain", M.Sc. Thesis in civil engineering, Texas Tech University, 1995.

[4] S. C. Tapia and R. Chellali, "Simple Kármán Street model," OCEANS'10 IEEE SYDNEY, Australia, 2010. https://doi.org/10.1109/oceanssyd.2010.5603671

[5] M.-J. Thoraval et al., "von Kármán Vortex Street within an Impacting Drop," Physical Review Letters, Vol. 108, Issue 26, 2012. https://doi.org/10.1103/physrevlett.108.264506

[6] S. Ali, S. Menenteau, Ch. Habchi, T. Lemenand, J.-L. Harion, and A. Elmarakbi, "Numerical analysis and simulation of the interaction between a von Kármán vortex street and elastic flaps" 21ème Congrès Français de Mécanique, Bordeaux, 26 au 30 août 2013.

[7] N. B. M. Noor, "Analysis of vortex shedding in a various body shapes", M.Sc. Thesis in mechanical engineering, faculty of mechanical and manufacturing engineering, Universiti Tun Hussein Onn Malaysia, 2015.

[8] X. Wang and S. Alben, "The dynamics of vortex streets in channels," Physics of Fluids, Vol. 27, Issue 7, 2015. https://doi.org/10.1063/1.4927462

[9] S. S. Dol, "Proper orthogonal decomposition analysis of vortex shedding behind a rotating circular cylinder," EPJ Web of Conferences, Vol. 114, p. 02019, 2016. https://doi.org/10.1051/epjconf/201611402019

[10] M. Heil, J. Rosso, A. L. Hazel, and Morten Brøns, "Topological fluid mechanics of the formation of the Kármán-vortex street," Vol. 812, pp. 199-221, 2016. https://doi.org/10.1017/jfm.2016.792

[11] S. Dai, B. A. Younis, H. Zhang, and C. Guo, "Prediction of vortex shedding suppression from circular cylinders at high Reynolds number using base splitter plates," Journal of Wind Engineering and Industrial Aerodynamics, Vol. 182, pp. 115-127, 2018. https://doi.org/10.1016/j.jweia.2018.09.006

[12] A. Morast, "Learning From the von Kármán Vortex Street", M.Sc. Thesis in Computational Sciences and Robotics, Faculty of South Dakota School of Mines and Technology, Rapid City, South Dakota, 2019.

[13] C. S. Greco, G. Paolillo, T. Astarita, and G. Cardone, "The von Kármán street behind a circular cylinder: flow control through synthetic jet placed at the rear stagnation point," Journal of Fluid Mechanics, Vol. 901, 2020. https://doi.org/10.1017/jfm.2020.427

[14] M. S. Ghazijahani, F. Heyder, J. Schumacher, C. Cierpka, "The von Kármán Vortex Street, an archetype for Machine Learning in turbulence", Symposium "Experimental Fluid Mechanics" 7-9 Sep. 2021. ISBN 978-3-9816764-7-1

[15] Z. Maches, E. Bartley, J. Borjon, and R. Carretero-González, "Stability of finite and infinite von Kármán vortex-cluster streets," Physical review, Vol. 103, Issue 3, 2021. https://doi.org/10.1103/physreve.103.032205

[16] F. Alzabari, C. A. M. E. Wilson, and P. Ouro, "Unsteady vortex shedding dynamics behind a circular cylinder in very shallow free-surface flows," Computers & Fluids, Vol. 260, pp. 105918-105918, 2023. https://doi.org/10.1016/j.compfluid.2023.105918

[17] J. S. Keeler and D. G. Crowdy, "Exact solutions for submerged von Kármán point vortex streets cotravelling with a wave on a linear shear current," Journal of Fluid Mechanics, Vol. 969, 2023. https://doi.org/10.1017/jfm.2023.551

[18] P. R. N. Childs, Rotating flow, Butterworth-Heinemann, Imperial College London, 2011. ISBN: 978-0-12-382098-3.

[19] C. H. K. Williamson, "Vortex Dynamics in the Cylinder Wake," Annual Review of Fluid Mechanics, Vol. 28, Issue 1, pp. 477-539, 1996. https://doi.org/10.1146/annurev.fl.28.010196.002401

[20] K. F. Liaw, "Simulation of Flow around Bluff Bodies and Bridge Deck Sections using CFD", Ph.D. thesis, Department of Civil Engineering, Faculty of Engineering, University of Nottingham, 2005. https://eprints.nottingham.ac.uk/id/eprint/10125

[21] I. W. Seo and C. G. Song, "Numerical simulation of laminar flow past a circular cylinder with slip conditions," International Journal for Numerical Methods in Fluids, Vol. 68, Issue 12, pp. 1538-1560, 2011. https://doi.org/10.1002/fld.2542